UJEAS

UNIZIK JOURNAL OF ENGINEERING AND APPLIED SCIENCES

UNIZIK Journal of Engineering and Applied Sciences 3(4), September (2024), 1272 - 1290
Journal homepage: https://journals.unizik.edu.ng/index.php/ujeas
PRINT ISSN: 2992-4383 || ONLINE ISSN: 2992-4391

Synthesis of Low-cost Ceramic microfiltration membrane with sawdust as pore former for brewery water purification

Ndubuisi Igboko [1*], Mathew Chukwudi Menkiti [2], Nkuzinna Ogbonna Chris[1] and Odebiyi Samuel Oluwasegun [3]

[1] Department of Chemical Engineering, School of Engineering and Engineering Technology, Federal University of Technology, Owerri, P.M.B 1526, Imo State, Nigeria

[2] Department of Chemical Engineering, Nnamdi Azikiwe University, P.M.B 5025, Awka, Nigeria

[3] Institute of Process Engineering of Chinese Academic of Sciences, Beijing 100190, PR China; University of Chinese Academy of Sciences, Beijing, PR China

[*]Corresponding Author's E-mail: ndubuisi.igboko@futo.edu.ng; mc.menkiti@unizik.edu.ng

Abstract

A flat microfiltration membrane was successfully developed using natural Nsu kaolinite clay and sawdust as a pore former through the solid-state method. The goal is to minimize dependence on costly imported sand and activated carbon filters for brewery water treatment. The membrane's preparation conditions, including kaolinite content, the optimal sintering conditions, including temperature and duration, were determined utilizing Response Surface Methodology (RSM) based on Box-Behnken design. The optimized membrane exhibited excellent properties, including high porosity (44.4%), permeability (1566.6 L/h/m²/bar), mechanical strength (35.97MPa), and suitable pore size (0.8332 µm). The membrane demonstrated exceptional purification performance when treating brewery borehole water, successfully eliminating turbidity, conductivity, TSS, and TDS to meet brewery quality requirements with rejection rates of 87.4%, 75%, 90%, and 75.9%, respectively. Additionally, the pH of the purified water fell within the acceptable range for brewery strike water, which tends to be neutral.

Keywords: Microfiltration, Nsukaolin, Response surface methodology, Strike water

1. Introduction

The brewing industry is a vital sector of the food industry, with a substantial global impact. Beer is a highly consumed beverage worldwide, a recent report from Global Data reveals Africa as the world's fastest-growing region for beer consumption. Nigeria leads Africa in beer consumption, with citizens drinking an average of 12.28 liters per person each year. Between 2015 and 2020, Africa's beer consumption is projected to grow at a 5% annual rate, surpassing Asia's 3%, the Middle East and North Africa's 2.8%, and Western Europe's less than 1%. This rapid growth solidifies Africa's position as the leading continent in beer consumption expansion (Nkamnebe, 2018). In Nigeria, the brewing industry holds significant economic importance. To meet the growing demand for beer, industry leaders and researchers are collaborating to develop innovative technologies that enable the production of high-quality beer at affordable prices.

Beer is predominantly water, comprising over 90% of its content. As a result, water quality plays a crucial role in brewing, influencing factors such as flavor, color, taste, and clarity. Its chemical properties impact every stage of production, including fermentation and preservation, making stringent water quality standards essential (Punčochářová et al., 2019).According Punčochářová et al, (2019), water quality standard Include Turbidity: 0-0.5

NTU, Dissolved solids: 20-50 mg/l, Suspended solids: 30-61 mg/l, pH: 5-9.5,Color: 0.00 PCU, Conductivity: 25-50 µS/cm.Ensuringhigh-quality water is crucial for producing excellent beer.

Water filtration membranes come in two main types: inorganic and polymeric. Ceramic and other inorganic membranes outperform polymeric membranes due to their exceptional mechanical strength, thermal resilience, chemical resistance, and long-lasting durability (Felix et al., 2015). Ceramic membranes come with a higher price tag due to the costly raw materials used, such as titania, zirconia, and alumina, and the complex manufacturing process involved (Amin et al., 2018).Researchers aim to make ceramic membranes more economically and environmentally viable by utilizing affordable materials and industrial waste. Examples include natural pozzolan for textile effluent treatment (Achiou et al., 2016) , bentonite clay for industrial effluents (Bouazizi et al., 2016), natural perlite for ceramic membranes in industrial wastewater treatment (Saja et al., 2018) , and clay/phosphate mixtures for seawater desalination and industrial wastewater pretreatment (Mouiya et al., 2018) . These studies demonstrate that leveraging local and natural resources to produce low-cost membranes is a viable and promising approach. This innovative approach maintains membrane excellence while reducing costs, promoting sustainability, and conserving resources.

Water purification using membranes has undergone substantial growth since the 20th century, driven by innovations in materials and design, expanding its applications across multiple sectors, notably in the brewing industry (Dong et al, 2022). Porous ceramic membrane (PCM) filtration has emerged as a leading technology for water treatment, offering a promising alternative for brewery water purification. PCMs can be fabricated using locally sourced biomass and clays, with various biomass sources like sawdust being used as pore formers to create the desired porosity. This study explores the use of sawdust, a waste biomass, as a pore former in ceramic membranes to enhance brewery water purification. By incorporating sawdust, the membrane's efficiency and sustainability are improved, allowing for higher water permeability, flux rates, and contaminant removal. Additionally, using sawdust reduces the need for costly ceramic materials, making the filtration system more economical

To further improve membrane performance, it's essential to optimize the experimental setup, which involves minimizing materials, energy, and time. Traditionally, experiments have used a one-factor-at-a-time approach, which is time-consuming and requires numerous trials. However, Response Surface Methodology (RSM) has gained popularity due to its efficiency in reducing trials and analyzing multiple factors simultaneously, including their interactions. Specifically, The Box-Behnken design-based Response Surface Methodology (RSM) is popular due to its efficiency, necessitating fewer experimental runs compared to a three-level full factorial design. This method surpasses central composite design in efficiency and avoids extreme experimental conditions, providing a more balanced approach (Ayaz et al,2020). Using the Box-Behnken design, researchers can optimize experimental conditions more effectively and efficiently. A comprehensive study investigated the critical parameters affecting ceramic filter performance, specifically the sawdust/clay ratio, furnace temperature, and firing time. Findings showed that porosity plays a crucial role in filtration rates, which can be optimized by modifying the sawdust/clay ratio and sawdust size. Moreover, firing temperature significantly influences filter properties and efficiency. Notably, research on kaolin-based ceramics showed that the mullite phase, crucial for ceramic strength, forms at temperatures above 900°C, with optimal development at 1000°C or higher (Soppe et al., 2015).

This research aims to develop a flat, porous ceramic microfiltration membrane using sawdust as a sustainable pore former and Kaolin clay. The primary application of this membrane will be to purify raw borehole water, transforming it into high-quality strike water that meets the stringent standards required for brewing. In essence, the goal is to create a membrane that can effectively treat natural water sources, making them suitable for use in the brewing process

2.0 Material and methods

2.1 Raw materials sourcing and Instrumental characterization

Kaolin clay was obtained from Obo Nzu (Agbara-nzu) in Ehime-Mbano, Imo State while Sawdust was obtained from Aboki timbers in Eziobodo, Owerri West Local Government, Imo State. The TGA/DTA was performed on the kaolin using a TGA instrument (Make TGA 4000 Perkin Elmer)to investigate the thermal transition during sintering. Before starting the experiment, the "measure sample" icon was chosen. Sample details such as the starting temperature, first temperature scan, first isothermal, and second temperature scan were inputted in the Method Editor. The TGA was allowed to run. The maximum operating temperature was 1200℃ and the maximumheat up rate was set at 20℃. When the measurement was complete, the kaolin was removed.

The XRD patterns were carried out in an XRD equipment (Miniflex 600) for the kaolin sample Research results are commonly presented in tables or x-y plots, showcasing two peak positions and corresponding X-ray counts (intensity). To determine relative intensity, the peak intensity is divided by the intensity of the dominant peak and multiplied by 100. The XRF characterization was performed with the Genius IF instrument, kaolin and sawdust samples were all involved here. The WinTrace software's Acquisition Manager was used to construct a Method Tray List that enabled automated quantitative analysis. The first sample identification/analysis was entered into the Method Tray List, and the Method File was selected from the directory. The next sample was input on the following line after Acquisition Management opened the Method File and confirmed the sample position in the tray as being accurate. This process went on until all of the samples had been used.

2.2 Preparation of sawdust cellulose

200g of sawdust was weighed into a 1000 ml conical flask,700ml10%w/vsodium hydroxide (NaOH) was poured into the flask and corked. The flask and its content were autoclaved at 121ºC at 15 psi for 30 minutes, after cooling the fibre material was washed using distilled water.500 ml of 5% hydrogen peroxide was added to the digested fibre and heated again at 100ºC for another 30minutes. The fibre was washed again using distilled water, 10% w/v sodium hypochlorite was added to the fibre (cellulose) to bleach it at 100ºC for 30 minutes. The cellulose was washed finally using deionized water to remove color and ions until the effluent water became clear. The washed cellulose was dried in the oven at 80ºC for 3hours, before increasing the temperature to 105 ℃for 2 hours for constant weight loss. The dried cellulose was ground and sieved using a standard sieve with a mesh size of 50 μm.

2.3 Membrane synthesis

The synthesis of porous ceramic membranes (PCMs) adopted here was the solid-state method described by Smart and Moore (2020) with modifications. Mixtures of kaolin and cellulose were measured in the ratio of 95%, 90%, and 85% kaolin and 5%, 10% and 15% sawdust respectively. Deionized water was subsequently added to the 1:1 kaolin-cellulose mixture to achieve a uniform consistency. The mixed samples were then cast in a prepared mold and oven-dried at 105℃ for 24 hours to form a disk membrane. The cast membranes were removed from the mold and transferred into the resistance muffle furnace. The membrane was calcined at 900℃, 1000℃ and 1100℃ for 1 hour, 2hours and 3hours based on the experimental runs specified in the box-behnken design. After formation, the membrane was cooled and submerged in water for 24 hours to fully saturate its pores and prevent cracking prior to testing. The porosity of the ceramic membrane was then determined using a saturated water method (Chen, 2018). In addition to other properties, the water permeability of the fabricated membrane was determined. The compressive strength was calculated by dividing the applied load (N) by the membrane's cross-sectional area (cm^2), yielding a value in N/cm^2.

2.4 Experimental Design and Procedure

To optimize membrane properties, a Box-Behnken design was employed, analyzing the effects of sintering temperature (A), duration (B), and mixture ratio (C) on porosity (P), water permeability (WP), and mechanical strength (MS). The required number of experiments (N) was determined using Eq. (1)

$$N = 2k(k-1) + R_o \quad (1)$$

In this equation, k represents the number of factors being studied, and R_O denotes the number of replicate experiments conducted at the center point of the experimental design. There are fifteen trials in total, three of which are duplicates of the center point. Table 1 shows clearly, the factors and their levels. The approach of least squares regression was utilized to model the experimental data. The regression model's applicability was evaluated using ANOVA and the model fit test. Furthermore, three-dimensional visuals illustrating the interplay among the variables were obtained. To ascertain the ideal set of operational parameters for the membrane production, membrane optimization was also conducted.

Table 1: Independent factors and their levels

Factor	Name	Units	Type	Subtype	Minimum	Maximum	Coded Low	Coded High	Mean	Std. Dev.
A	Temp	^{0}C	Numeric	Continuous	900.00	1100.00	-1 ↔ 900.00	+1 ↔ 1100.00	1000.00	75.59
B	Time	Hr	Numeric	Continuous	1.0000	3.00	-1 ↔ 1.00	+1 ↔ 3.00	2.00	0.7559
C	mixture ratio	%wt	Numeric	Continuous	5.00	15.00	-1 ↔ 5.00	+1 ↔ 15.00	10.00	3.78

2.5 Determination of membrane properties

2.5.1 Water permeability

Water permeability tests were performed using a dead-end filtration system, where PCMs prepared under various conditions were subjected to a constant pressure of 0.08 mPa. Distilled water filtration was used to determine permeability, with permeate flux Jw, ($Lh^{-1}m^{-2}$) and permeability coefficient Lp, ($Lh^{-1}m^{-2}bar^{-1}$) calculated using equations (2) and (3)

$$\text{Permeate flux } (J_w) = \frac{V}{A.t} \quad (2)$$

while permeability is given as

$$\text{Permeability } (L_p) = \frac{J_w}{\Delta P} \quad (3)$$

Where V (L) represents the volume of water passing through the membrane, the time t in hours (h), A (m^2) represents the surface area of the filtration and ΔP in bar (bar) represents the transmembrane pressure.

2.5.2 Pore volume and porosity

A saturated water method is used to determine the porosity of PCMs. The water-saturated mass of the membrane was determined by weighing a dry sample, soaking it in water for 24 hours, and then re-weighing it. The pore volume and porosity were subsequently calculated using equations (4) and (5).

$$\text{Pore Volume} = \frac{\text{mass of wet membrane (Mw)} - \text{mass of dry membrane (Md)}}{\text{density of water}} \quad (4)$$

$$\text{Porosity} = \frac{\text{Pore volume of the membrane}}{\text{Total volume of the membrane}} \times 100 \quad (5)$$

2.5.3 Mechanical strength

For mechanical strength evaluation, rectangular membrane samples with identical surface area and thickness to the flat disk membrane were prepared. The flexural mechanical strength was then assessed using a 1 kN Shimadzu Screw Flat Grips system, complying with ASTM C674-88 standards, based on a three-point bending load calculation outlined in equation (6) as

$$\text{Mechanical strength (MS)} = \frac{3PL}{2bd^2} \quad (6)$$

In this equation, P (N) denotes the maximum rupture load, L (mm) is the support span, and b (mm) and d (mm) represent the sample's width and thickness, respectively.

2.5.4 Microfiltration test

The optimized membrane's efficiency was evaluated through filtration of raw borehole water from Golden Guinea Breweries, Umuahia, Abia State, Nigeria, at 0.08 mPa pressure. Pre- and post-filtration characterization of the water assessed pH, turbidity, color, conductivity, total dissolved solids (TDS), and total suspended solids (TSS), enabling calculation of rejection rates (Rx%) for each parameter using equation (7).

$$R_x = \left(1 - \frac{X_p}{X_f}\right) \times 100 \quad (7)$$

Where X_f represents the initial characterization parameters (before filtration, or feed), and Xp represents the final characterization parameters after filtration, or product. The optimized samples underwent scanning electron microscopy (SEM) analysis using a PhenomProX SEM (Phenom World, Einhoven, Netherlands) to examine physical structural changes. Sample preparation involved gold coating (5nm) via Qorum Technologies' Q150R sputter coater, mounted on a double adhesive sample stub. After initial focusing and adjustments using NaVCaM, the sample was transferred to SEM mode for final focusing and automatic brightness/contrast adjustment, followed by capturing morphological images at various magnifications on a USB drive .ASTME 2809 (2022) was partly followed here. FTIR and XRD procedure was also carried out on the optimized membrane sample.

3.0 Results and Discussions

3.1 Thermal analysis of the Kaolin (Nsu Clay) (TGA/DTA)

Thermal analysis is used to identify the temperature ranges where kaolin undergoes significant weight loss and transformation. To understand the thermal degradation behavior of kaolin, its porous structure, pore diameter, and mechanical strength are evaluated at various temperature regimes. The thermal analysis results, shown in Fig. 1, reveal a complex, nonlinear relationship. The kaolin sample loses approximately 75.2% of its weight between 25.5°C and 884.8°C, with two distinct weight loss stages. The first stage, occurring between 25.5°C and 270°C, is primarily due to the loss of physisorbed water. The second stage, between 320°C and 610°C, corresponds to the dehydroxylation of kaolinite, transforming it into an amorphous metakaolin phase. The DTA curve shows an endothermic peak at 380°C, indicating this transformation, and an exothermic peak between 600°C and 635°C, related to the crystallization of spinel (Hubadillah *et al*., 2018)

$$Al_2O_3.2SiO_2.2H_2O(\text{kaolinite}) \rightarrow Al_2O_3.2SiO_2(\text{metakaonite}) + 2H_2O \quad (8)$$

According to the TGA curve, the material demonstrated thermal stability beyond 843°C, with no substantial weight loss observed. This indicates that a minimum sintering temperature of 843°C is necessary for optimal membrane production, ensuring superior performance and durability

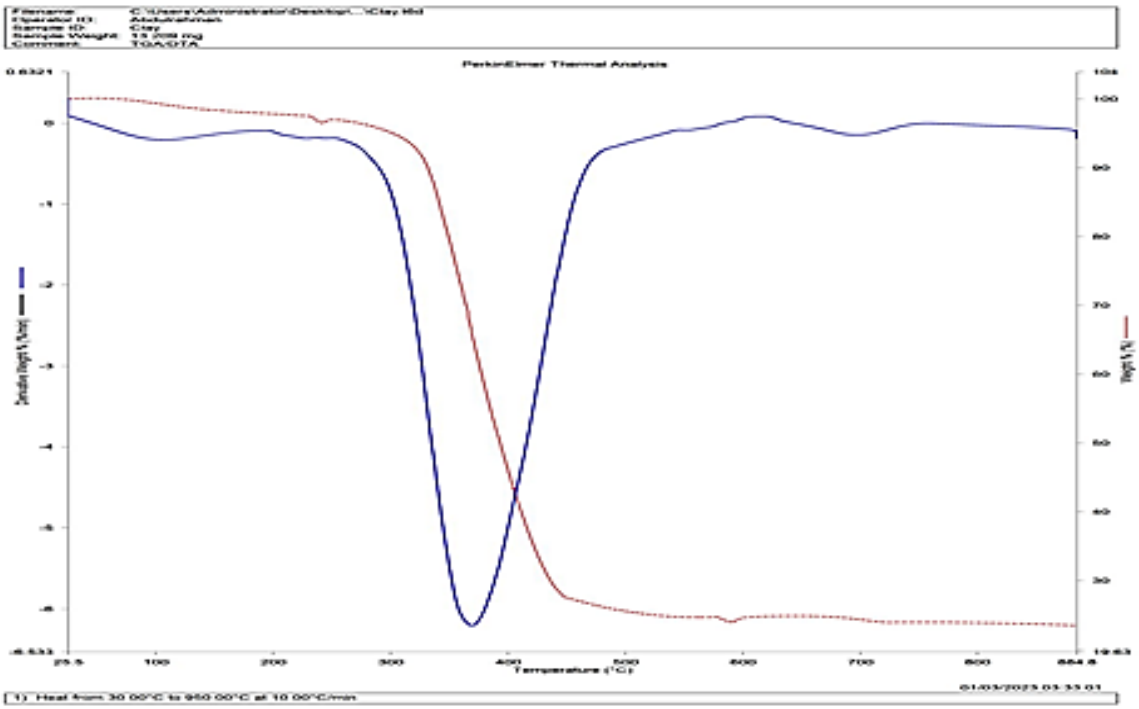

Fig.1:TDA/DTA of Nsukaolin

3.2 Characterization by XRD analysis

The TGA-DTA analysis shows that essentially no substantial weight loss occurred above the sintering temperature of 884°C. An XRD investigation of clay structure at a temperature greater than 884 °C is performed to support this claim. Peaks and trends in the XRD chart in Figure 2showedthat the inorganic mixture's primary constituents are mainly quartz, kaolinite, nacrite and illitewith peaks of 467.52cts at 26.777º2Th, 83.26cts at 12.51º2Th,32.11cts at 39.59 º2Th and 69.90cts at 24.18º2Th respectively, the structural changes that appeared on the Nsukaolin is awell-defined diffractions of kaolin clay at 2 theta values of 11.18-13.8°, 19.55-20.9°, and 24.8° commonly associated with kaolinite (Aragaw and Angerasa, 2020; Senoussi *et al*., 2016). However, the peaks corresponding to the 2 Theta values of 21.5° and 27.6° are typical quartz properties (Douiri *et al*., 2017). Behnamfard*et al*. (2019) established that kaoline mineralogical makeup contains quartz, which raises the silicon dioxide (SiO_2) level. In ceramic bodies and glazes, enormous amounts of quartz powder in the form of $SiO_2$are employed. Quartz particles often behave as an embedded aggregate in bodies by remaining unmodified in the fired matrix. In porcelain bodies, they serve as the "skeleton", this property is a huge advantage in membrane production. No additional substantial phase shift occurs above 850 °C, according to a critical inspection of the peaks at higher temperatures. Metakaolinite, a metastable phase of alumina-silica formed by heating kaolinite, makes up the majority of the membrane's skeletal structure. It is also clear from the XRD analysis that sintering temperatures above 850 °C are enough for membrane formation.

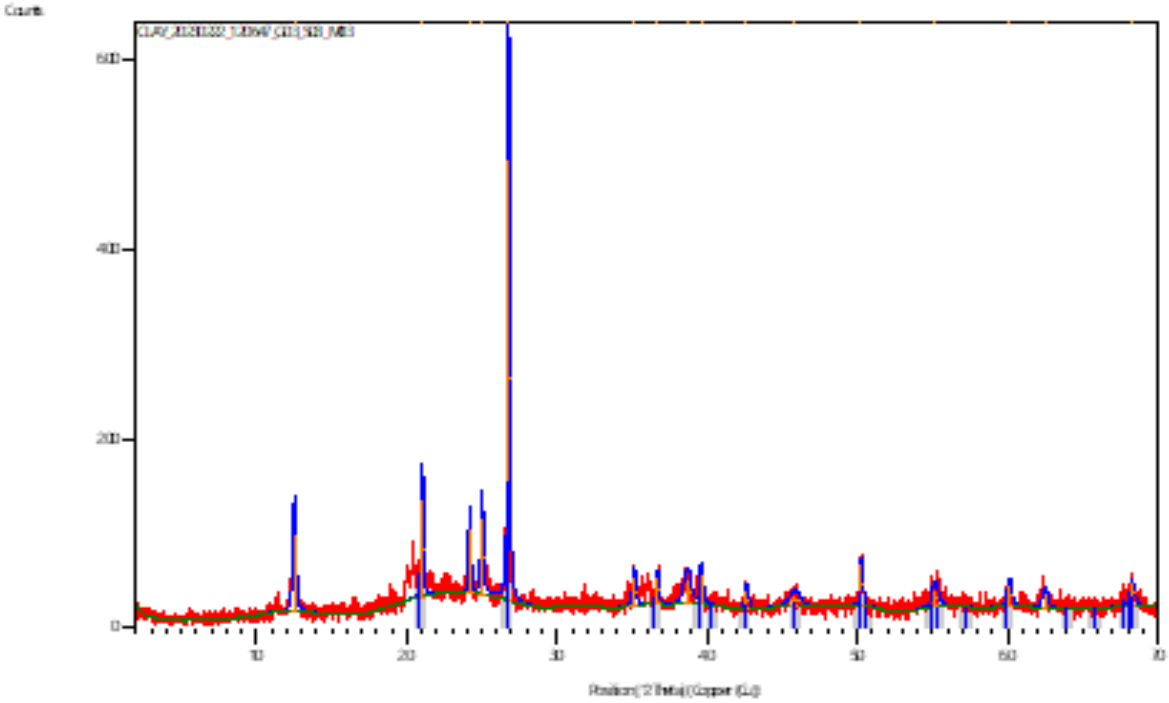

Fig. 2:X-ray diffraction (XRD) patterns of Nsukaolin

3.3 XRF Characterization of Nsu Clay (kaolin)

According to the results of an X-ray fluorescence (XRF) analysisshown in Table 2 below, Nsu clay has high concentrations of SiO_2 (79.06 weight percent), significant concentrations of Al_2O_3 (10.05 weight percent), significant concentrations of SO_3 (3.48 weight percent) and Fe_2O_3 (2.90 weight percent), and lower concentrations of Cl (1.35 weight percent), CaO (1.34 weight percent), and TiO_2 (1.12 weight percent). K_2O, ZnO, and CuO are in negligible amounts.

Table 2: Chemical composition of Nsukaolin

Composition	Al_2O_3	SiO_2	SO_3	Fe_2O_3	Cl	CaO	TiO_2	K_2O	ZnO	CuO
Wt %	79.06	10.05	3.48	2.90	1.35	1.34	1.12	0.206	0.149	0.076

Garcia-Valles et al. (2020) stated that the Al_2O_3/Fe_2O_3 mass ratio may be utilized to identify, from an industrial perspective, the possible final uses of the clays in the formation of ceramic paste. Because of its greater Al_2O_3/Fe_2O_3 ratio and lower iron oxide content, Nsu kaolin serves as a viable, cost-effective raw material for producing ceramic membranes suitable for water filtration applications, with its Aluminum and Iron oxide content contributing to improved colloidal stability.

3.4 XRF characterization of sawdust

It is significant to know that the behavior of sawdust is influenced by its chemical makeup. Hemicellulose, cellulose, and lignin are the three main chemical components of sawdust. These vaporizes completely at elevated temperatures with the evolution of CO_2 whose escape creates pores required in membrane fabrication. The elemental contents of sawdust are listed in Table 4.2 below.

Table 3 Chemical constituents (in %) of the sawdust.

Chemical Compositions (%)					
CaO	Cl	SiO_2	Al_2O_3	Fe_2O_3	LOI
58.55	16.03	14.72	7.95	1.08	4.76

According to Faheem and Sobolev (2014), a high calcium oxide (lime) content is a sign of strong bond strength. The effectiveness of sawdust as a cement replacement relies on its chemical profile, including the presence and amounts of silica, alumina, iron, and calcium oxide. These cement-like properties are what is needed in ceramic membrane fabrication.

Determination of appropriate model

Table 4 shows the three factors of the Box-Behnken design and the corresponding responses from experiments. Examining the several models to identify the ones that best fit the experimental data allowed us to find the right model for predicting porosity, permeability, and mechanical strength.

Table 3: Three factors of the Box-Behnken design and the responses to them

		Factor 1	Factor 2	Factor 3	Response 1	Response 2	Response 3
Std	Run	A:Temp ^oC	B:Time hr	C:mixture ratio %wt	Porosity	Water Permeability	Mechanical Strength
9	1	1000	1	5	36.5	1350	18.3
15	2	1000	2	10	33	1140	15
13	3	1000	2	10	35.3	1179	16
12	4	1000	3	15	33.8	940	32
2	5	1100	1	10	42.1	1421	12.3
6	6	1100	2	5	44.0	1409	24.5
4	7	1100	3	10	40.5	1528	30.6
5	8	900	2	5	41.5	1920	17.3
7	9	900	2	15	29.5	530	16.5
1	10	900	1	10	31.3	769	8.48
10	11	1000	3	5	41.6	1780	30.0
14	12	1000	2	10	34	1170	16.5
8	13	1100	2	15	39.3	1675	28.
3	14	900	3	10	37	1364	10.2
11	15	1000	1	15	33.4	958	19

The importance of the values of the model equations for porosity, water permeability and mechanical strength was examined by F, R^2, adjusted R^2, lack-of-fit and adequate precision tests. For porosity, as shown in Table 6, the model F-value, which is normally evaluated by dividing the mean squares of each variable response by the mean square, was 8.34, and a low probability value of 0.1116, which was less than the p-value at the 95% confidence limit, signifies that the model terms were significant. The model probability value of 0.0038 for water permeability and 010129 for mechanical strength also came out as low, enough to confirm that the model terms for water permeability and mechanical strength were significant. The models' accuracy was further evaluated using the R^2 correlation coefficient, which measures the strength of the relationship between the selected variables and the proportion of parameter variability explained (Raposo & Barcelo, 2021).

Table 5 showed that the R^2 value of 0.9722 for porosity indicated that only 0.028% of the variation in the porosity response could not be explained by the model and the model fitted well with the observed data. The R^2 values of 0.9916 and 0.9904 for water permeability and mechanical strength respectively were also reasonably close to unity, therefore acceptable. The adjusted R^2 values for porosity, water permeability and mechanical strength were obtained as 0.9222, 0.9764 and 0.9731 respectively were all statistically reasonable. Lack-of-fit tests in Table 6 were also used to evaluate the model adequacy; an insignificant lack-of-fit is required here. The lack-of-fit values for porosity, water permeability and mechanical strength were 0.3442, 0.0638 and 0.2058 respectively; these values were statistically insignificant and showed that the constructed models were consistent with the observations. The values of adequate precision displayed in Table 7 indicated that the signal-to-noise ratios were 13.45, 29.81 and 22.51 for porosity, water permeability and mechanical strength respectively, the values being greater than 4 indicating a robust, significant and reliable signal. Fig. 3 shows that the points of the predicted vs. actual plots for porosity, water permeability and mechanical strength observations were aligned along a diagonal line, showing a strong correlation between predicted and observed values.

Table 4: Summary of model fit results for membrane properties

			Porosity			
Source	**Std. Dev.**	**R^2**	**Adjusted R^2**	**Predicted R^2**	**PRESS**	
Linear	2.67	0.7131	0.6348	0.4778	142.94	
2FI	2.41	0.8306	0.7036	0.4856	140.79	
Quadratic	**1.23**	**0.9722**	**0.9222**	**0.6888**	**85.19**	**Suggested**
Cubic	1.15	0.9903	0.9320		*	Aliased
			Permeability			
Source	**Std. Dev.**	**R^2**	**Adjusted R^2**	**Predicted R^2**	**PRESS**	
Linear	285.77	0.5531	0.4312	0.0621	1.885E+06	
2FI	113.49	0.9487	0.9103	0.8077	3.865E+05	
Quadratic	**58.22**	**0.9916**	**0.9764**	**0.8708**	**2.597E+05**	**Suggested**
Cubic	20.42	0.9996	0.9971		*	Aliased
			MS			
Source	**Std. Dev.**	**R^2**	**Adjusted R^2**	**Predicted R^2**	**PRESS**	

Linear	5.39	0.6023	0.4938	0.2036	639.86	
2FI	5.54	0.6941	0.4647	-0.3964	1121.89	
Quadratic	**1.24**	**0.9904**	**0.9731**	**0.8664**	**107.37**	**Suggested**
Cubic	0.7638	0.9985	0.9898		*	Aliased

Table 5: Summary of Lack of fit test results for membrane properties

			Porosity			
Source	**Sum of Squares**	**Df**	**Mean Square**	**F-value**	**p-value**	
Linear	77.30	9	8.59	8.34	0.1116	
2FI	43.98	6	7.33	7.12	0.1283	
Quadratic	**2.99**	**3**	**0.9975**	**0.9684**	**0.3442**	**Suggested**
Cubic	0.0000	0				Aliased
			Permeability			
Source	**Sum of Squares**	**Df**	**Mean Square**	**F-value**	**p-value**	
Linear	9.947E+05	9	1.105E+05	265.47	0.0038	
2FI	1.229E+05	6	20481.89	49.20	0.0201	
Quadratic	**18525.75**	**3**	**6175.25**	**14.83**	**0.0638**	**Suggested**
Cubic	0.0000	0				Aliased
			MS			
Source	**Sum of Squares**	**Df**	**Mean Square**	**F-value**	**p-value**	
Linear	**320.72**	**8**	**40.09**	**77.10**	**0.0129**	**Suggested**
2FI	240.40	5	48.08	92.46	0.0107	
Quadratic	**4.01**	**2**	**2.01**	**3.86**	**0.2058**	**Suggested**
Cubic	0.0000	0				Aliased

Table 6: Adequate Precision

Porosity	Water permeability	Mechanical Strength

13.45	29.81	22.51

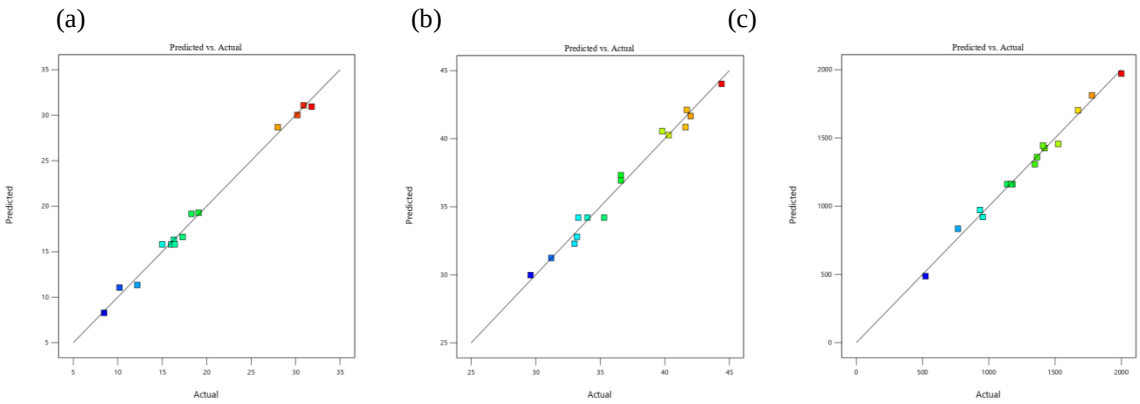

Fig. 3: Graphical representation for the models (a) Porosity (b) water permeability (c) mechanical strength.

The accuracy of the membrane property models was confirmed by comparing them to experimental data from a three-factor Box-Behnken design, exposing the relationships between input variables and predicted results. Multiple regression analysis (Table 8) enabled model calibration and parameter estimation, yielding equations (9), (10), and (11) for porosity, water permeability, and mechanical strength, respectively

$$\text{Porosity} = +303.3 - 0.554250\text{A} + 19.05\text{B} - 5.1\text{C} - 0.018250\text{AB} + 0.003650\text{AC} - 0.235\text{BC} + 0.000294\text{A}^2 + 0.6875B^2 + 0.0615\text{C}^2 \quad (9)$$

$$\text{WP} = +17129 - 27.4275\text{A} + 1621.25\text{B} - 924.9\text{C} - 1.22\text{AB} + 0.828\text{AC} - 22.4\text{BC} + 0.0117\text{A}^2 - 9.5B^2 + 4.14\text{C}^2 \quad (10)$$

$$\text{MS} = -93.097 + 0.318083\text{A} - 42.133\text{B} - 8.21367\text{C} + 0.041450\text{AB} + 0.002150\text{AC} + 0.065\text{BC} - 0.000184A^2 + 1.406B^2 + 0.3034\text{C}^2 \quad (11)$$

These equations were used to predict the porosity, water permeability and mechanical strength of the membrane properties.

Table 7: Regression terms for porosity

Factor	Coefficient Estimate	Degree of Freedom	Sum of squares	F-value	P-value
Intercept	+303.30000	1	266.11	F-value	p-value
A-Temperature	-0.554250	1	88.44	19.43	0.0022
B-Time	+19.05000	1	11.52	58.11	0.0006
C-Mixture ratio	-5.10000	1	95.22	7.57	0.0403
AB	-0.018250	1	13.32	62.56	0.0005
AC	+0.003650	1	13.32	8.75	0.0316
BC	-0.235000	1	5.52	8.75	0.0316
A^2	+0.000294	1	31.86	3.63	0.1151

B^2	+0.687500	1	1.75	20.93	0.0060
C^2	+0.061500	1	8.73	1.15	0.3332

Table 8: Regression terms for water permeability

Factor	Coefficient Estimate	Degree of Freedom	Sum of squares	F-value	P-value
Intercept	+17129.00000	1	1.993E+06	65.35	0.0001
A-Temperature	-27.42750	1	2.628E+05	77.55	0.0003
B-Time	+1621.25000	1	1.551E+05	45.77	0.0011
C-Mixture ratio	-924.90000	1	6.938E+05	204.73	< 0.0001
AB	-1.22000	1	59536.00	17.57	0.0086
AC	+0.828000	1	6.856E+05	202.30	< 0.0001
BC	-22.40000	1	50176.00	14.81	0.0120
A^2	+0.011700	1	50544.00	14.91	0.0119
B^2	-9.50000	1	333.23	0.0983	0.7665
C^2	+4.14000	1	39552.92	11.67	0.0189

Table 9: Regression terms for mechanical strength

Factor	Coefficient Estimate	Degree of Freedom	Sum of squares	F-value	P-value
Intercept	-93.09667		795.73	57.31	0.0002
A-Temperature	+0.318083	1	230.27	149.27	< 0.0001
B-Time	-42.13333	1	249.98	162.05	< 0.0001
C-Mixture ratio	-8.21367	1	3.64	2.36	0.1849
AB	+0.041450	1	68.72	44.55	0.0011
AC	+0.002150	1	4.62	3.00	0.1440
BC	+0.065000	1	0.4225	0.2739	0.6231
A^2	-0.000184	1	12.56	8.14	0.0357
B^2	+1.40583	1	7.30	4.73	0.0816
C^2	+0.303433	1	212.47	137.73	< 0.0001

3.5 Analysis of variance

Table 11 presents the ANOVA results for the models related to porosity, water permeability, and mechanical strength of the produced membrane. A p-value less than 0.05 indicates that a model term is significant and reliable for prediction, suggesting that changes in the corresponding physical factor values can substantially impact the response. Conversely, model terms with p-values greater than 0.1 are considered non-significant, according to Asfaram et al. (2016), indicating that variations in the related physical element values do not significantly affect the response.

Table 10: Analysis of variance for porosity, permeability and mechanical strength

Response	Variation source	Df	Sum of squares	Mean square	F-ratio	P-values
Porosity	Regression	9	266.11	29.57	19.43	0.0022
	Residual	5	5	1.52		
	Total	14	271.11	31.09		
WP	Regression	9	1993000	221500	65.35	0.0001
	Residual	5	16945.00	3389		
	Total	14	2009945	224889		
MS	Regression	9	795.73	88.41	57.31	0.0002
	Residual	5	7.71	1.54		
	Total	14	803.44	89.95		

3.6 3D surface plots for interaction.

Three-dimensional response surface plots, as noted by Coimbra et al., (2016), effectively illustrate the relationships between two variables while keeping the third constant, revealing individual and interactive effects. These plots, along with their corresponding contour plots, provide a clear and intuitive visualization of how experimental variables impact responses, facilitating easier analysis and interpretation. To gain a deeper understanding of how independent variables and their interactions influence the dependent variable, this study generated 3D response surfaces based on model equations (8-10). These visual representations showcase the relationships, with curvatures resulting from the quadratic polynomial order. Gradient colors represent continuous changes in the response variable, with hotspots indicating maximum or minimum responses, depicted by bright colors or sharp color changes, ranging from blue (minimum) to red (maximum) in this study. To better understand how the dependent and independent variables relate, contour plots were created. Since the regression model has three independent variables, one variable was fixed at its center level for each plot. This resulted in 3D response plots and three corresponding contour plots for porosity, water permeability, and mechanical strength, as shown in Figure 4.According to Figure 4, variation of sintering temperature from 900℃ to 1100℃leads to the increase of porosity (a) and permeability (b). However, this increase is more significant at a high level of the amount of rice husk (15wt%) (from 28.3% to 40.5% for porosity and from 499 to 1750 $Lh^{-1}m^{-2}bar^{-1}$ for permeability compared to the increase at a low level (5wt %) where the porosity slightly increases from 41.2% to 43.1% and permeability decreases from 1750 to 1400 $Lh^{-1}m^{-2}bar^{-1}$.The reverse is the case for mechanical strength which slightly increased at low level (5 wt %)(c). This significant increase in porosity and water permeability suggested that sawdust is a pore former. They burn during the sintered membrane process, creating pores. For permeability, they open pores and raise membrane flow, so an increase in the number of pores directly affects permeability. A similar observation was made by Samhari, et al. (2020). Since sawdust created greater room after burning, it is evident that higher sawdust content improves the porosity of PCMs. Higher porosity was anticipated to increase the water filtration flow rate, but regrettably, it resulted in a major decrease in the mechanical strength at 28.2MPa.The creation of closure between pores, which

results in the densification phenomena that is expected at this temperature range, could account for the decreased water permeability (Beqqour *et al*., 2019).

When the mixture ratio is low, extending the sintering time from 1 to 3 hours substantially enhances permeability and moderately boosts porosity. Specifically, porosity increases from 33.5% to 42%, while water permeability jumps from 1000 to 17500 $Lh^{-1}m^{-2}bar^{-1}$.This demonstrates that further sintering leads to a good phase rearrangement and robust grain connection as observed by Beqqour *et al*.,(2019). However, for mechanical strength, a higher value of 30MPa was recorded (f). According to Dung et al (2021), the quantity of sawdust used as a pore-forming agent significantly influences ceramic membrane porosity, with higher porosity potentially compromising mechanical strength. Thus, optimizing membrane performance requires balancing porosity and strength.

There is a significant rise in mechanical strength from 10.2 to 32.7MPa as a result of the variation in sintering temperature from 900 to 1100 ℃at high sintering time of 3hours(g). Additionally, there is a moderate increase in permeability and a poor increase in porosity at these conditions. This anticipated behavior is mostly caused by the high degree of densification that occurs over time under the influence of sintering along with a significant strengthening of the connections between grains (Mohamed *et al*., 2019). On the other hand, when the sintering temperature is varied at a low level (1hour), it results in a slight increase in mechanical strength from 5.2 to 11.6MPa and a significant increase in porosity from 26.7% to 41.9% (i), a strong increase in permeability from 350 to 1320 $Lh^{-1}m^{-2}bar^{-1}$(h) Partial densification brought on by the brief sintering period within the same temperature range may account for this.

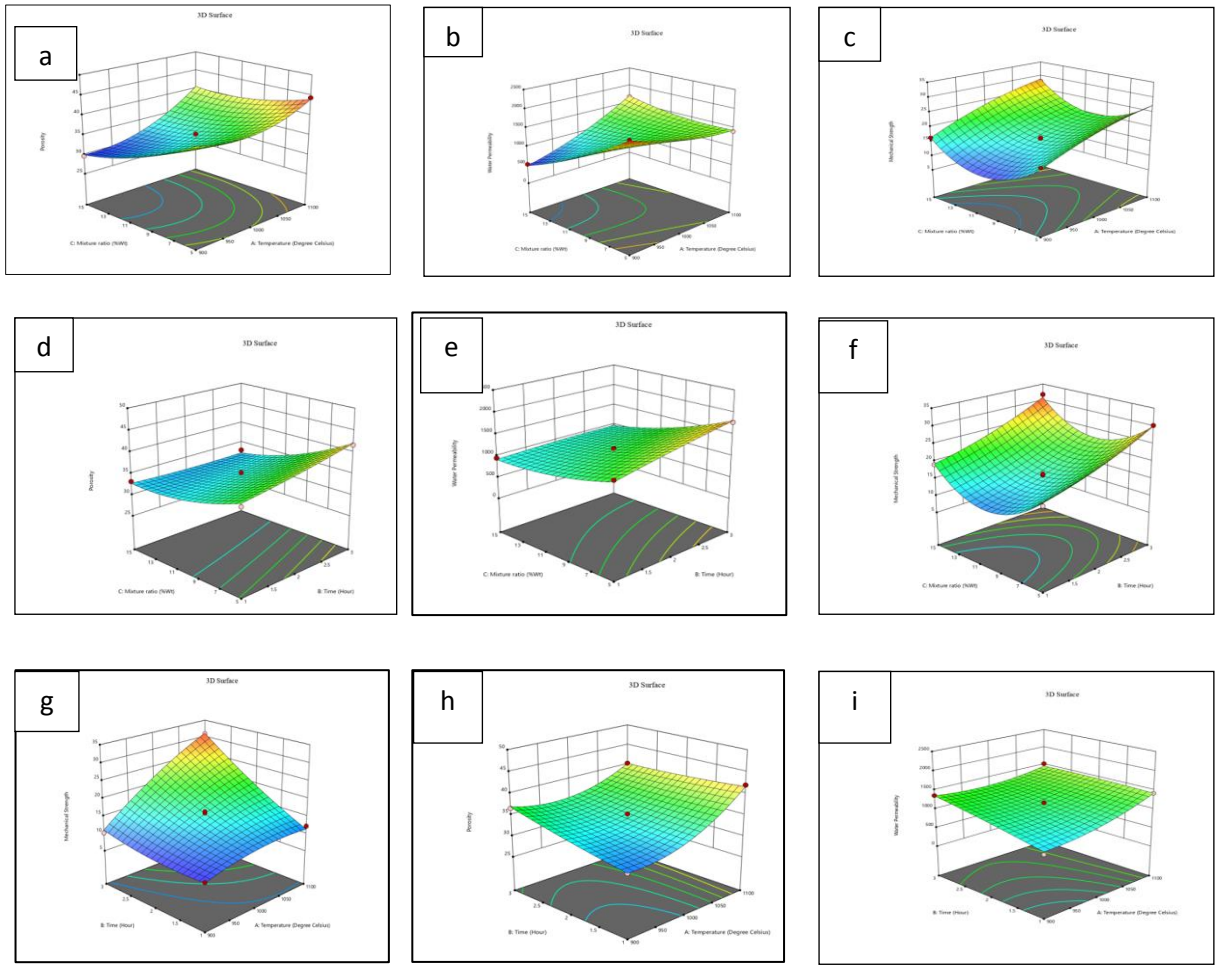

Fig. 5:3D surface plots for porosity, water permeability and perfunctory strength of membranes

3.7 Optimization.

When interacting terms vary, they can have opposing effects on different responses, with positive impacts on one response and negative impacts on another. This indicates that optimal conditions differ across regions for various responses. Consequently, due to limitations in visualizing optimal conditions through 3D surface plots, the desirability function is utilized to pinpoint ideal settings. Tables 12 and 13 outline the input factor boundaries and individual desirability functions for porosity, water permeability, and mechanical strength of PCMs. Optimal ceramic filter performance requires high mechanical strength, porosity, and permeability. This forms the basis for constraints as shown in Table 12 for the desired responses.

Table 11: Table of constraints for optimization

Name	Goal	Lower Limit	Upper Limit	Lower Weight	Upper Weight	Importance
			Factors			
A:Temperature	is in range	900	1100	1	1	3
B:Time	is in range	1	3	1	1	3
C:Mixture ratio	is in range	5	15	1	1	3
			Responses			
Porosity	maximize	29.6	44.4	1	1	3
Water Permeability	maximize	522	2000	1	1	3
Mechanical Strength	maximize	8.46	31.8	1	1	3

Table 12: Individual desirability functions for porosity, water permeability and mechanical strength

Number	Temperature	Time	Mixture ratio	Porosity	Water Permeability	Mechanical Strength	Desirability	
1	**1085.084**	**3.000**	**5.000**	**44.000**	**1585.611**	**35.257**	**0.912**	**Selected**
2	1086.117	3.000	5.000	44.048	1584.005	35.311	0.912	
3	1085.753	2.986	5.000	44.000	1582.736	35.125	0.912	
4	1087.360	3.000	5.089	44.000	1577.694	35.144	0.910	
5	1087.193	2.954	5.002	44.000	1576.511	34.832	0.910	

Completely intended responses include high porosity, water permeability and mechanical strength. The optimal conditions in coded values for the mixture ratio, sintering temperature, and sintering duration are − 1, 1 and 1 respectively. It was discovered that the desirability is equal to 0.912. The equivalent true values for the kaolinite quantity, sintering temperature, and sintering duration are 5%, 1100℃, and 3 hours, respectively. To verify the optimal points obtained, validation experiments were conducted under conditions outlined. The predicted and actual results were then compared, and residual and percentage error values were calculated and presented in Table 14. The highest value of porosity, water permeability and mechanical strength was 44.4%, 1566 L h^{-1} m^{-2} $bar^{-1}$and 35.97 MPa respectively while the validation experiments gave 45.9%, 1563.7 L h^{-1} m^{-2} $bar^{-1}$and 36.5 MPa. The errors (%) between the predicted and observed response values were acceptable and were within 4%.

Table 13: Optimization results

Max. Response	Temp.	MR	Time	Pred. Response	Obs. Response	Error
Porosity	1100℃	5%	3hrs	44.0%	43.8%	0.2
Permeability	1100℃	5%	3hrs	$1585.6Lh^{-1}m^{-2}bar^{-1}$	$1587.7Lh^{-1}m^{-2}bar^{-1}$	2.1
Mech. Strength	1100℃	5%	3hrs	35.25 MPa	35.30 MPa	0.05

3.8 Characterization of the optimized membrane

Using X-ray diffraction, the phase change brought on by the rising firing temperature was investigated. The findings are displayed in Figure 5. Peaks at 36.5º, and 42.4º represent the mullite phase's diffraction. Previous studies have shown that mullite formation occurs at temperatures exceeding 900°C (De Aza et al., 2014; González-Miranda et al., 2018), and it plays a significant role in the development of mechanical strength in ceramics (Olanrewaju *et al*., 2019; Heraiz *et al*., 2016).These findings explain why ceramics' compressive strength increases at high firing temperatures such as 1100°C. FTIR spectra of the membrane show the condensation of Si-OH and the thermal breakdown of sawdust as displayed in Figure 6. Following firing at 1100°C, a notable vibration at 1062.3 cm^{-1} and 2158.5 cm^{-1}, corresponding to C-H bonding and the -OH group in the membrane vanished, suggesting the burning out of sawdust. And the peak at 779 cm^{-1}indicates the condensation of Si-OH groups (Dung *et al*., 2021). According to Zewedie et al (2021), FTIR was employed to identify the crystal structures, and functional groups existing in the membrane, it can also detect other structural anomaly that may be present in the prepared membrane. Hydroxyl groups on the membrane surface play a crucial role in forming hydrogen bonds, serving as both donors and acceptors, which influences the purification process.

SEM micrographs of the top view of a sawdust/kaolinite optimized membrane with 500, 1000 and 2000 magnifications are displayed in Fig. 7. SEM images made it evident that the membrane was well-sintered and has a porous structure that corresponds with the porosity result. This showed that the particles have been well-consolidated, resulting in a largely uniform surface morphology. According to Zou et al (2019), the development of necks between grains promotes high cohesion between them, which accounts for the good mechanical strength of the optimized membrane and capacity to withstand hydraulic pressure during microfiltration.This process also shows the aggregation of particles, resulting in a more compact and dense ceramic body. Using ImageJ software, the pore size of the sawdust/kaolinite optimized membrane was estimated on sixseparate top-view SEM images (Quaddari *et al*., 2019; He *et al*., 2020).Fig.8 displays the pore size distribution of the membrane. The membrane surface has holes that are found to be between 0.2 and 3.1 µm in diameter, this shows that the fabricated membrane is well positioned in the MF range. The average pore size was found to be 0.8332 µm.

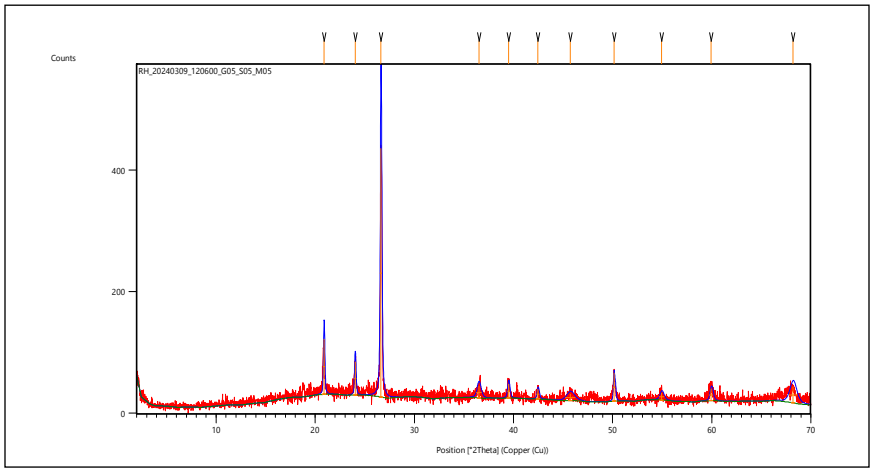

Fig. 6: XRD of Optimized Koalinite/sawdust membrane

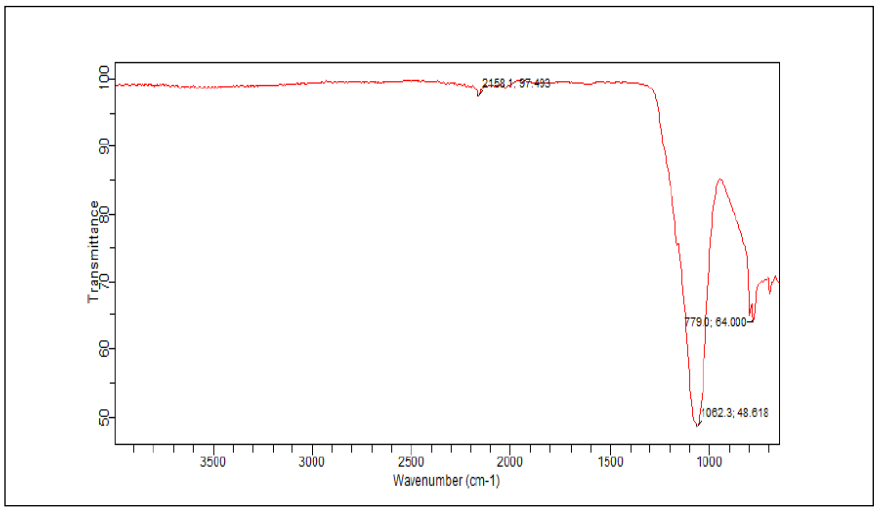

Fig. 7: FTIR representation of the optimized membrane

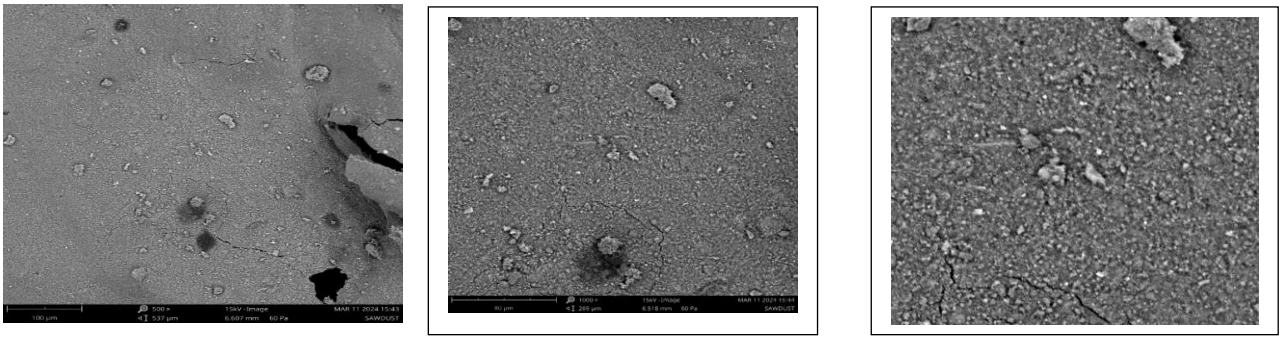

Fig. 8: SEM micrograph of Optimized membrane

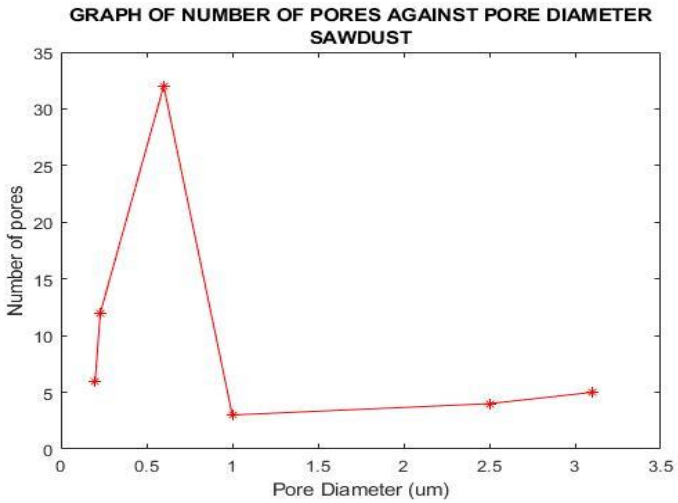

Fig. 9: Pore size distribution of the optimized membrane

3.9 Purification of Brewery water (Strike water)

Table 15 shows the physicochemical parameters of the brewery water before and after the microfiltration (MF) experiment. The ideal ranges for brewing water properties are: turbidity (0-0.5 NTU), dissolved solids (20-50mg/l), suspended solids (30-61mg/l), pH (5-9.5), color (0.00 PCU), and conductivity (25-50μS/cm). The taste of beer is substantially affected by the pH and mineral profile of its water, regardless of beer style. Notably, alkaline brewing water can disrupt extraction and impair beer quality (Punčochářová, 2019). The results in Table 15 show that the pH was neutralized before mashing. Minerals in the water, such as calcium, magnesium, carbonates, sulfates, and sodium, contribute to the beer's flavor. The water's hardness, measured by total dissolved calcium and magnesium (TDS), was within the acceptable range (28mg/l). Turbidity, TSS, and conductivity were also within acceptable limits, indicating good water quality for brewing. Visual inspection showed that the water had a neutral color, suitable for brewing. The Nsu kaolinite/sawdust membrane successfully removed 87.4% of turbidity, 75% of TDS, 90% of TSS, and 75.9% of conductivity, demonstrating its effectiveness in purifying brewery water. For years, membrane technology has been applied in brewing for various solid-liquid separations, complementing or replacing traditional techniques. Membrane separation offers numerous benefits, including efficient removal of microorganisms and molecules, reduced thermal effects, lower energy consumption, and flexible design. Applications include raw water treatment, brewing processes, and wastewater management, with microfiltration being the most widely used method.

Table 14: Physicochemical characterization of Brewery water

Brewery water	pH	Turbidity	Color	TDS	TSS	Conductivity
Before	6.84	3.10	ND	104	590	160
After	6.87	0.39	ND	26	58.2	38.6
Rejection (%)	–	87.4	ND	75.0	90	75.9

4.0. Conclusion

Solid state procedure was used to create an affordable ceramic MF membrane by combining kaolinite and rice husk. RSM based on Box-Behnken design was utilized to examine the impact of experimental membrane fabrication parameters and their interactions. The optimum membrane was made with 5% kaolinite and sintered for 3 hours at 1100 ◦C. Its porosity, permeability and mechanical strength are 44.4, 1566 L h^{-1} m^{-2} $bar^{-1}$and 35.97MPa respectively. Moreover, homogenous and defect-free microstructure was shown by SEM characterization. Lastly, the filtering of borehole water into Strike water was used to evaluate the effectiveness of the membrane. Its capacity to eliminate turbidity, TDS, TSS and conductivity was verified, yielding rejection rates of 87.4%, 75%, 90%, and 75.9% respectively. These results demonstrate that borehole water could be purified into brewery Strike water using the low-cost ceramic MF membrane that was synthesized. Membrane separation technology shows great potential in beer brewing in the future, offering improvements in beer quality through either replacement or integration with traditional methods.

5.0 Recommendation

Industries, especially breweries should adopt a developed and green process that would incorporate membrane technology in water purification. The use of Membrane Separation Processes (MSPs) shows great potential and can enhance or even replace traditional treatment methods as they can be applied either as a substitute or as a supplementary step to augment the already existing procedure. This, as has been shown, will greatly increase efficiency.

It is also recommended that other agricultural and plant waste be incorporated as this will combat pollution.

Acknowledgements

The authors are thankful to New Concept laboratories (NCL), Owerri, Imo state and Golden Guinea breweries Plc, Abia State, Nigeria for their support.

Nomenclature

PCM = Porous ceramic membrane;
RSM = Response surface methodology;
MF = Microfiltration;
RH = Rice husk;

K = Number of factors;
RO = Number of replicates;
Jw = Permeate flux($Lh^{-1}m^{-2}$);
L_p = Permeability($Lh^{-1}m^{-2}bar^{-1}$);
ΔP (bar) = Trans membrane pressure;
$X_f$and Xp = Characterization parameters before (feed) and after (product) filtration, respectively;
TSS = Total suspended solids (mg/l);
TDS = Total dissolved solids (mg/l);

References

Achiou, B., Elomari, H., Ouammou, M., Albizane, A., Bennazha, J., Younssi, S. A., & Aaddane, A. 2016. Elaboration and characterization of flat ceramic microfiltration membrane made from natural Moroccan pozzolan (Central Middle Atlas). J. Mater. Environ. Sci, 7(1), 196-204.

Amin, S. K., Roushdy, M. H., and El-Sherbiny, C. A. 2016. An overview of production and development of ceramic membranes.

Aragaw, T. A., and Angerasa, F. T. 2020. Synthesis and characterization of Ethiopian kaolin for the removal of basic yellow (BY 28) dye from aqueous solution as a potential adsorbent. *Heliyon*, *6*(9).

Asfaram, A., Ghaedi, M., Azqhandi, M. A., Goudarzi, A., and Dastkhoon, M. J. R. A. 2016. Statistical experimental design, least squares-support vector machine (LS-SVM) and artificial neural network (ANN) methods for modeling the facilitated adsorption of methylene blue dye. *RSC advances*, *6*(46), 40502-40516.

Ayaz Atalan, Y., Tayanç, M., Erkan, K., & Atalan, A. 2020. Development of nonlinear optimization models for wind power plants using box-Behnken design of experiment: A case study for Turkey. Sustainability, 12(15), 6017.

Behnamfard, A., Chegni, K., Alaei, R., and Veglio, F. 2019. The effect of thermal and acid treatment of kaolin on its ability for cyanide removal from aqueous solutions. *Environmental earth sciences*, *78*, 1-12.

Belgada, A., Charik, F. Z., Achiou, B., Kambuyi, T. N., Younssi, S. A., Beniazza, R., and Ouammou, M. 2021. Optimization of phosphate/kaolinite microfiltration membrane using Box–Behnken design for treatment of industrial wastewater. *Journal of Environmental Chemical Engineering*, *9*(1), 104972.

Beqqour, D., Achiou, B., Bouazizi, A., Ouaddari, H., Elomari, H., Ouammou, M., and Younssi, S. A. 2019. Enhancement of microfiltration performances of pozzolan membrane by incorporation of micronized phosphate and its application for industrial wastewater treatment. *Journal of Environmental Chemical Engineering*, *7*(2), 102981.

Bouazizi, A., Saja, S., Achiou, B., Ouammou, M., Calvo, J. I., Aaddane, A., & Younssi, S. A. 2016. Elaboration and characterization of a new flat ceramic MF membrane made from natural Moroccan bentonite. Application to treatment of industrial wastewater. Applied Clay Science, 132, 33-40.

Chen, H., & Yang, B. 2018. Experiment and simulation method to investigate the flow within porous ceramic membrane. Journal of the Australian Ceramic Society, 54, 575-586.

Coimbra, D. B., Martins, R. M., Neves, T. T., Telea, A. C., & Paulovich, F. V. 2016. Explaining three-dimensional dimensionality reduction plots. Information Visualization, 15(2), 154-172.

De Aza, A. H., Turrillas, X., Rodriguez, M. A., Duran, T., & Pena, P. 2014. Time-resolved powder neutron diffraction study of the phase transformation sequence of kaolinite to mullite. Journal of the European Ceramic Society, 34(5), 1409-1421.

Dong, Y., Wu, H., Yang, F., & Gray, S. 2022. Cost and efficiency perspectives of ceramic membranes for water treatment. Water Research, 220, 118629.

Douiri, H., Louati, S., Baklouti, S., Arous, M., and Fakhfakh, Z. 2017. Structural and dielectric comparative studies of geopolymers prepared with metakaolin and Tunisian natural clay. *Applied Clay Science*, *139*, 40-44..

Dung, T. T. N., Nam, V. N., Nhan, T. T., Hoang, B. N., Hung, D. L. T., and Quang, D. V. 2021. Utilization of Rice Husk, an Abundant and Inexpensive Biomass in Porous Ceramic Membrane Preparation: A Crucial Role of Firing Temperature. *Journal of Nanomaterials*, *2021*(1), 8688238.

Farrow, C., McBean, E., Huang, G., Yang, A., Wu, Y., Liu, Z., and Li, Y. 2018. Ceramic water filters: A point-of-use water treatment technology to remove bacteria from drinking water in Longhai City, Fujian Province. *Journal of Environmental Informatics*, *32*(2), 63-68.

Felix, A., Herdegen, V., Haseneder, R., Härtel, G., and Repke, J. U. 2015. Investigations on the behaviour of ceramic micro-and mesoporous membranes at hydrothermal conditions. *Separation and Purification Technology*, *148*, 85-93.

Garcia-Valles, M., Alfonso, P., Martínez, S., and Roca, N. 2020. Mineralogical and thermal characterization of kaolinitic clays from Terra Alta (Catalonia, Spain). *Minerals*, *10*(2), 142..

González-Miranda, F. D. M., Garzón, E., Reca, J., Pérez-Villarejo, L., Martínez-Martínez, S., & Sánchez-Soto, P. J. 2018. Thermal behaviour of sericite clays as precursors of mullite materials. Journal of Thermal Analysis and Calorimetry, 132, 967-977.

He, X., Xu, W., Ding, F., Xu, C., Li, Y., Chen, H., and Shen, J. 2020. Reaction-based ratiometric and colorimetric chemosensor for bioimaging of biosulfite in live cells, zebrafish, and food samples. *Journal of Agricultural and Food Chemistry*, *68*(42), 11774-11781.

Heraiz, M., Sahnoune, F., Hrairi, M., Saheb, N., and Ouali, A. 2016. Kinetics of mullite formation from kaolinite and boehmite. *Molecular Crystals and Liquid Crystals*, *628*(1), 55-64.

Hubadillah, S. K., Othman, M. H. D., Matsuura, T., Ismail, A. F., Rahman, M. A., Harun, Z. and Nomura, M. 2018. Fabrications and applications of low cost ceramic membrane from kaolin: A comprehensive review. *Ceramics International*, *44*(5), 4538-4560.

Mohamed Bazin, M., Ahmad, N., and Nakamura, Y. 2019. Preparation of porous ceramic membranes from Sayong ball clay. *Journal of Asian Ceramic Societies*, *7*(4), 417-425.

Moore, E. A., and Smart, L. E. 2020. Optical properties of solids. In *Solid State Chemistry* (pp. 283-314). CRC Press.Van Halem, D. (2006). Ceramic silver impregnated pot filters for household drinking water treatment in developing countries. *Delft University of Technology*, *1*.

Mouiya, M., Abourriche, A., Bouazizi, A., Benhammou, A., El Hafiane, Y., Abouliatim, Y., & Hannache, H. 2018. Flat ceramic microfiltration membrane based on natural clay and Moroccan phosphate for desalination and industrial wastewater treatment. Desalination, 427, 42-50.

Nkamnebe, A. D., Ahmed, M. B., & Uzoka, L. O. 2018. Alcohol Consumption Regulation in Nigeria and National Development. LEADERSHIP, SECURITY AND NATIONAL DEVELOPMENT, 412.

Olanrewaju, A., Oluseyi, A. K., and Das, S. K. 2019. The effect of MgO and Cr2O3 on mullite formation from Nigeria sourced kaolin-calcined alumina sintered compacts. In *IOP Conference Series: Materials Science and Engineering* (Vol. 509, No. 1, p. 012007). IOP Publishing.

Ouaddari, H., Karim, A., Achiou, B., Saja, S., Aaddane, A., Bennazha, J., ... and Albizane, A. 2019. New low-cost ultrafiltration membrane made from purified natural clays for direct Red 80 dye removal. *Journal of Environmental Chemical Engineering*, *7*(4), 103268.

Punčochářová, L., Pořízka, J., Diviš, P., & Štursa, V. 2019. Study of the influence of brewing water on selected analytes in beer. Slovak Journal of Food Sciences/Potravinarstvo, 13(1).

Raposo, F., & Barcelo, D. 2021. Assessment of goodness-of-fit for the main analytical calibration models: Guidelines and case studies. TrAC Trends in Analytical Chemistry, 143, 116373.

Saja, S., Bouazizi, A., Achiou, B., Ouammou, M., Albizane, A., Bennazha, J., & Younssi, S. A. 2018. Elaboration and characterization of low-cost ceramic membrane made from natural Moroccan perlite for treatment of industrial wastewater. Journal of environmental chemical engineering, 6(1), 451-458.

Samhari, O., Younssi, S. A., Rabiller-Baudry, M., Loulergue, P., Bouhria, M., Achiou, B., and Ouammou, M. 2020. Fabrication of flat ceramic microfiltration membrane from natural kaolinite for seawater pretreatment for desalination and wastewater clarification. *Desalin. Water Treat*, *194*, 59-68.

Senoussi, H., Osmani, H., Courtois, C., and el Hadi Bourahli, M. 2016. Mineralogical and chemical characterization of DD3 kaolin from the east of Algeria. *boletín de la sociedad española de cerámica y vidrio*, *55*(3), 121-126.

Soppe, A. I. A., Heijman, S. G. J., Gensburger, I., Shantz, A., Van Halem, D., Kroesbergen, J., & Smeets, P. W. M. H. 2015. Critical parameters in the production of ceramic pot filters for household water treatment in developing countries. Journal of Water and Health, 13(2), 587-599.

Yue, X., Koh, Y. K. K., and Ng, H. Y. 2015. Effects of dissolved organic matters (DOMs) on membrane fouling in anaerobic ceramic membrane bioreactors (AnCMBRs) treating domestic wastewater. *Water Research*, *86*, 96-107.

Zewdie, T. M., Prihatiningtyas, I., Dutta, A., Habtu, N. G., and Van der Bruggen, B. 2021. Characterization and beneficiation of Ethiopian kaolin for use in fabrication of ceramic membrane. *Materials Research Express*, *8*(11), 115201.

Zou, D., Qiu, M., Chen, X., Drioli, E., and Fan, Y. 2019. One step co-sintering process for low-cost fly ash based ceramic microfiltration membrane in oil-in-water emulsion treatment. *Separation and Purification Technology*, *210*, 511-520